



Multiscale Imaging Approach for Studying the Central Nervous System: Methodology and Perspective

Michela Fratini^{1,2*}, Ali Abdollahzadeh³, Mauro DiNuzzo¹, Raimo A. Salo³, Laura Maugeri¹, Alessia Cedola², Federico Giove^{1,4}, Olli Gröhn³, Jussi Tohka³ and Alejandra Sierra³

¹ IRCCS Fondazione Santa Lucia, Rome, Italy, ² Institute of Nanotechnology-CNR c/o Physics Department, Sapienza University of Rome, Rome, Italy, ³ A. I. Virtanen Institute for Molecular Sciences, University of Eastern Finland, Kuopio, Finland, ⁴ Museo Storico della Fisica e Centro Studi e Ricerche Enrico Fermi, Rome, Italy

OPEN ACCESS

Edited by:

Ofer Pasternak,
Harvard Medical School,
United States

Reviewed by:

Diana Cash,
King's College London,
United Kingdom
Ayal Ben-Zvi,
The Hebrew University of Jerusalem,
Israel

*Correspondence:

Michela Fratini
michela.fratini@gmail.com

Specialty section:

This article was submitted to
Brain Imaging Methods,
a section of the journal
Frontiers in Neuroscience

Received: 09 September 2019

Accepted: 20 January 2020

Published: 07 February 2020

Citation:

Fratini M, Abdollahzadeh A, DiNuzzo M, Salo RA, Maugeri L, Cedola A, Giove F, Gröhn O, Tohka J and Sierra A (2020) Multiscale Imaging Approach for Studying the Central Nervous System: Methodology and Perspective. *Front. Neurosci.* 14:72. doi: 10.3389/fnins.2020.00072

Non-invasive imaging methods have become essential tools for understanding the central nervous system (CNS) in health and disease. In particular, magnetic resonance imaging (MRI) techniques provide information about the anatomy, microstructure, and function of the brain and spinal cord *in vivo* non-invasively. However, MRI is limited by its spatial resolution and signal specificity. In order to mitigate these shortcomings, it is crucial to validate MRI with an array of ancillary *ex vivo* imaging techniques. These techniques include histological methods, such as light and electron microscopy (EM), which can provide specific information on the tissue structure in healthy and diseased brain and spinal cord, at cellular and subcellular level. However, these conventional histological techniques are intrinsically two-dimensional (2D) and, as a result of sectioning, lack volumetric information of the tissue. This limitation can be overcome with genuine three-dimensional (3D) imaging approaches of the tissue. 3D highly resolved information of the CNS achievable by means of other imaging techniques can complement and improve the interpretation of MRI measurements. In this article, we provide an overview of different 3D imaging techniques that can be used to validate MRI. As an example, we introduce an approach of how to combine diffusion MRI and synchrotron X-ray phase contrast tomography (SXPCT) data. Our approach paves the way for a new multiscale assessment of the CNS allowing to validate and to improve our understanding of *in vivo* imaging (such as MRI).

Keywords: multimodal image coregistration, magnetic resonance image, X-ray phase contrast microtomography, multiscale imaging, brain, spinal cord, image coregistration

Abbreviations: 2D, two-dimensional; 3D, three-dimensional; ANTs, advanced normalization tools; CNS, central nervous system; dMRI, diffusion magnetic resonance imaging; DTI, diffusion tensor imaging; EM, electron microscopy; ESRE, european synchrotron radiation facility; FA, fractional anisotropy; LM, light microscopy; MRI, magnetic resonance imaging; SCT, spinal cord toolbox; SXPCT, synchrotron X-ray phase contrast tomography.

INTRODUCTION

Diagnosis, monitoring, surgical interventions, and treatment planning strategies of diseases in the central nervous system (CNS) strongly benefit from non-invasive imaging methods. Among all imaging techniques, magnetic resonance imaging (MRI) has become the most valuable approach in both clinical and experimental settings because of its non-invasive nature and high image quality. Conventional MRI sequences, such as T1- or T2-weighted, are extensively used to detect tissue alterations and damage during neurodegeneration, tumor growth or after injury. However, conventional MRI methods have low sensitivity for distinct early pathological processes. Other MRI methodologies, such as magnetization transfer (Filippi and Rocca, 2004, 2007; Sled, 2018), proton density (Mezer et al., 2016), susceptibility weighted imaging (Liu et al., 2015; Vargas et al., 2018), and diffusion MRI (dMRI) (Andre and Bammer, 2010; Cohen et al., 2017) are increasingly used in the imaging of the CNS. Diffusion MRI methods, such as diffusion tensor imaging (DTI) (Basser et al., 1994), can obtain tissue microstructural information and unveil tissue changes often not detectable by conventional MRI methods. Even though DTI is already an established and widely used tool, dMRI continues to develop, generating new acquisition approaches such as high-angular resolution diffusion imaging (Tuch et al., 2002), q-space imaging (Cohen and Assaf, 2002; Jensen et al., 2005) or multidimensional dMRI (Westin et al., 2016; Topgaard, 2017), and more elaborate models for data analysis (Wedeen et al., 2008; Panagiotaki et al., 2012; Zhang et al., 2012). These advanced dMRI methods have a great potential to extract intravoxel microstructural information in the CNS beyond DTI.

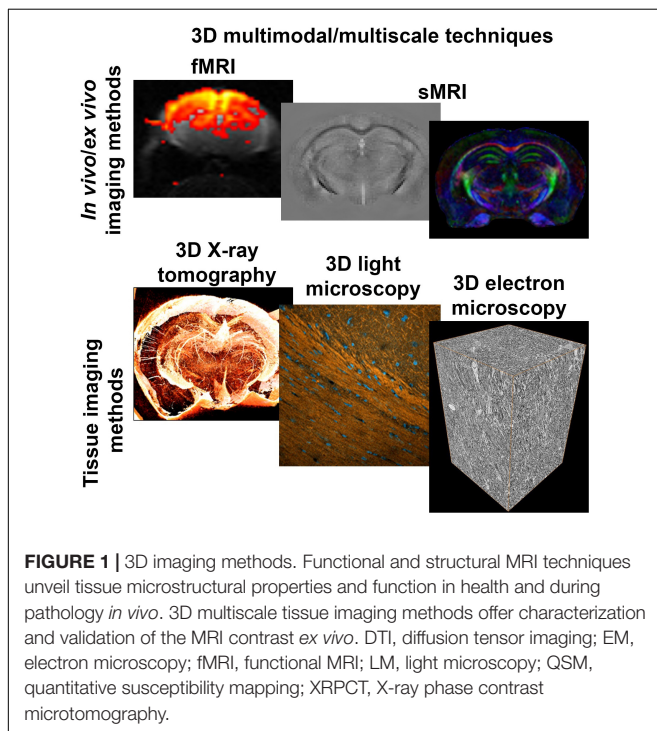
Other emerging MRI methods, such as quantitative susceptibility mapping (Schweser et al., 2011), can detect and discriminate between diamagnetic and paramagnetic materials, which is useful in conditions such as demyelination, calcifications or iron accumulation (Wang and Liu, 2015; Li et al., 2016; Aggarwal et al., 2018).

Despite the inherent value of structural and microstructural MRI techniques to detect abnormal tissue in the CNS, there is a lack of understanding of the origin of imaging contrast. The interpretation of MRI is a challenge because of the limited resolution, and leads us to question: *What information does a single voxel of MRI contain?* To answer this question, it is necessary to understand which tissue components dictate the MRI signal in each voxel. This level of understanding can be reached by correlating MRI contrast with underlying cellular components and characterizing the potential changes altering MRI signal. Therefore, the validation of MRI requires multimodal and multiscale imaging studies, from macro- to nanometer scale, with techniques able to show high-specificity and high-resolution tissue properties, such as cell somas, neurites, vessels, among others, and also in three-dimensional (3D) (Figure 1).

HIGH RESOLUTION IMAGING METHODS TO VALIDATE THE MRI CONTRAST

Traditionally, the validation of the MRI contrast has been done with *ex vivo* tissue preparations, e.g., employing histochemistry and immunohistochemistry, which are essentially two-dimensional (2D) approaches. Recent technological advances allow to image the tissue in high-resolution and in 3D with the possibility to image large tissue volumes (Figure 1). In particular, technological advances in light microscopy (LM) can image the tissue by optical sectioning of thick tissue sections (Helmstaedter et al., 2008). Confocal microscopes can image a tissue section up to 100 μm -thick (Stelzer, 2006). Tissue sections thicker than 100 μm can be imaged with more advanced techniques, such as light sheet microscopy (Weber and Huisken, 2011) or two-photon microscopy (Denk et al., 1990). Also, the resolution of LM methods have been improved in novel super-resolution techniques, such as stimulated-emission-depletion microscope reaching 40 nm planar resolution *ex vivo* (Hell and Wichmann, 1994) or structured illumination microscopy up to 100 nm resolution *in vivo* (Gustafsson, 2000). Additionally, tissue clearing techniques (Du et al., 2018), such as CLARITY (Chung et al., 2013), 3DCISCO (Ertürk and Bradke, 2013) or ScaleS (Hama et al., 2015), which make the tissue transparent and minimize light-scattering, have opened new avenues in the optical 3D imaging of large tissue coverage, e.g., whole brain.

Imaging of tissue ultrastructure can be achieved with electron microscopy (EM). Advanced EM techniques have expanded the applicability of EM by offering 3D imaging of large field-of-view of tissue (Briggman and Bock, 2012). Serial sectioning transmission EM methods can achieve nanometer in-plane resolution of large tissue sample by combining transmission EM with physical serial sectioning of the samples (Kreshuk et al., 2014). Automatic section-collection methods, such as



automated tape-collection ultramicrotome (Schalek et al., 2011), avoid laborious manual cutting of thousands of sections, image alignment, and missing/distorted sections. Other serial sectioning methods, such as serial block-face scanning electron microscopy (SBEM) can reduce tissue distortions by imaging the slice prior to sectioning (Denk and Horstmann, 2004). SBEM provides 3D high-resolution images collected at the mesoscopic scale in the order of a few hundred micrometers. Focused ion beam scanning electron microscopy (Heymann et al., 2006) is another 3D block-face EM technique (Heymann et al., 2006), which can achieve 4 nm resolution in-plane.

Conventional 3D X-ray imaging techniques, such as classical radiography and tomography (the most widely used tools for imaging objects with hard X-rays), are based on absorption contrast (i.e., on the imaginary part of the refraction index) and are obtained by measuring the attenuation of X-rays through the object. Conversely, high-resolution synchrotron X-ray phase contrast tomography (SXRPT) (Fratini, 2018) achieves the contrast by imaging the phase modulation induced by an object in a coherent beam, exploiting the real part of the complex refractive index (Fratini et al., 2015). In particular, SXRPT enables the simultaneous 3D visualization of both dense (e.g., bone) and soft objects (e.g., soft tissue) at length scales ranging from millimeters down to hundreds of nanometers, without the use of contrast agent, sectioning or destructive preparation of the samples (Fitzgerald, 2000; Stefanutti et al., 2018). Samples for XRPCT are typically prepared by perfusing with saline solution containing heparin (50 U/ml) followed by dissection, fixation in 4% paraformaldehyde, and storage in alcohol [for more details about the sample preparation see Fitzgerald (2000) and Stefanutti et al. (2018)].

Phase contrast makes SXRPT attractive for studies of weakly absorbing samples, both in materials and life sciences. In particular, the highest sensitivity of SXRPT to electron density with respect to conventional CT has allowed evaluating the morphological alterations in the vascular and the neuronal networks in animal models of neurodegenerative diseases such as multiple sclerosis and Alzheimer's disease (Bravin et al., 2012; Russo, 2017).

In the last decades, many X-ray phase contrast techniques have been developed and successfully applied. Such techniques permit to convert the phase variations of an X-ray beam, due to its interactions with the sample, in measurable intensity modulations.

A simple yet effective phase contrast method for hard X-rays is based on in-line imaging after free-space propagation, which does not require any additional optics, leading to source-limited rather than optics-limited resolution (Paganin et al., 2002). When X-rays illuminate the sample, variations in optical-path length produce slight local deviations (refraction) of the X-ray beam from its original path. When a free-space propagation distance is allowed between sample and detector, the recorded image contains the refraction information in the form of interference fringes, whose detectability depends on the coherence of the X-ray beam. Synchrotron-radiation X-ray sources provide high-photon flux X-ray beams, with a high degree of spatial coherence and allow for the possibility of providing monochromatic beams

(Weitkamp et al., 2011). The high quality of the images helps optimize the algorithms used for image analysis and the 3D reconstruction. For the reconstruction of the SXRPT volume, the first step is the phase retrieval which is applied to all projections of the tomographic measurements, using the code ANKAphase (Cedola et al., 2017; Massimi et al., 2019). The algorithm produces the projected thickness of the object, which is proportional to the refractive index decrement if the object is homogeneous. When applied to all tomographic projections, the retrieved phase maps can be fed to a standard filtered back-projection algorithm to obtain phase tomogram.

In summary, 3D high-resolution imaging methods can provide the necessary tissue information to validate the MRI contrast. LM, EM and X-ray imaging techniques offer 2D/3D high-resolution images, tissue specificity and sample coverage needed to understand the MRI signal in the healthy and diseased brain and spinal cord. Information regarding cell density or which type of cells are present in a particular area, density and orientation of axons forming fiber bundles, vascular density, shape and tortuosity, or any alteration in those tissue metrics during pathological processes can shed light into the interpretation of MRI parameters. Still, the challenge is to combine multidisciplinary and multiscale information into the same reference frame, which is the first step for analyses and quantification of areas of interest in the brain and spinal cord.

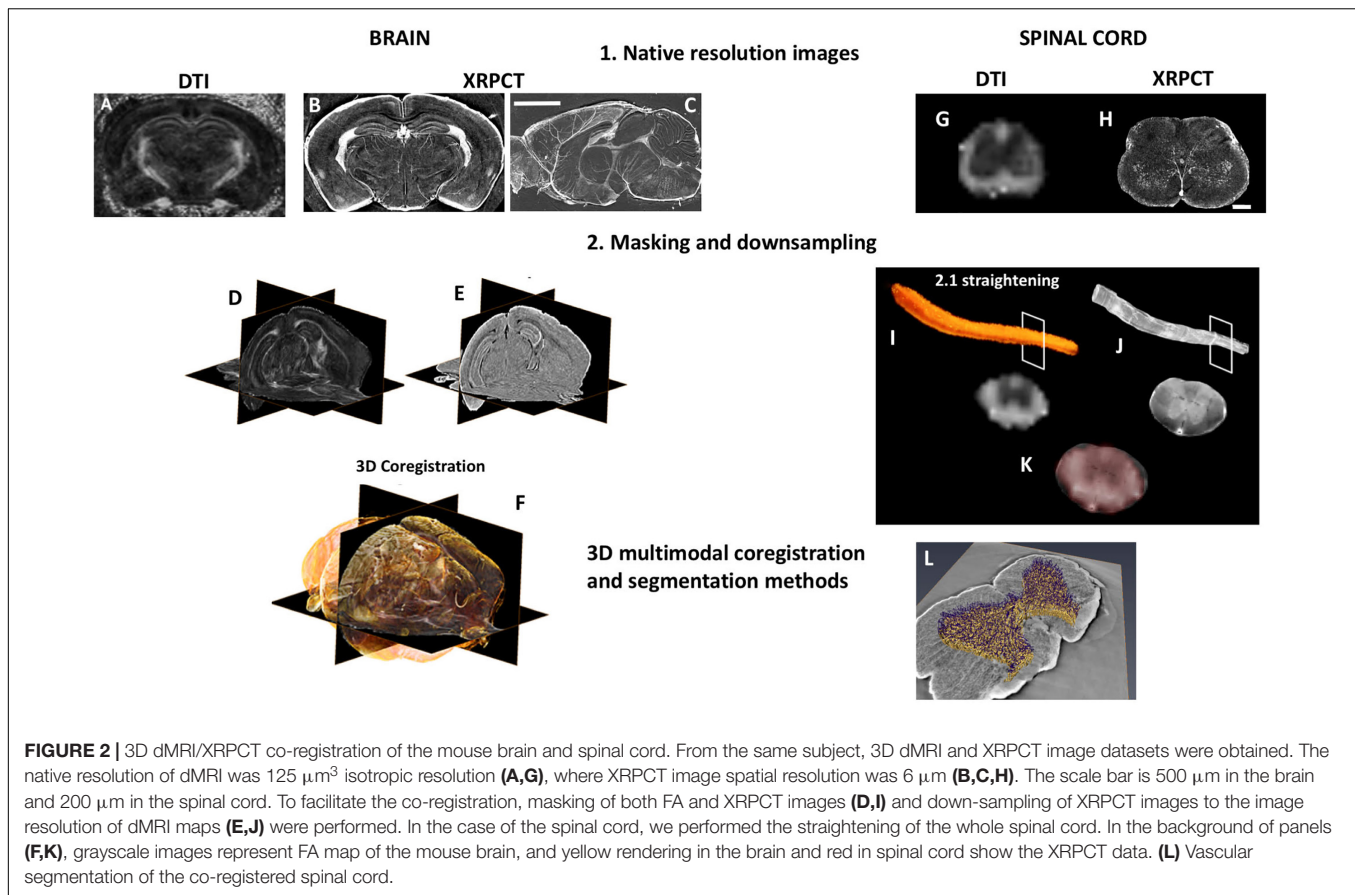
Therefore, more sophisticated co-registration tools are required to combine the MRI and tissue data into the same reference frame.

These microscopic techniques (nominal resolution of the order of one micron) could help providing a better interpretation of the images obtained with *in vivo* techniques, using higher-resolution images as a reference atlas.

Thus, from the co-registration between MRI, which has a nominal resolution of the order of 100 μm , and microscopic images, with a nominal resolution of the order of 1 μm , we can achieve information on the underlying microstructure influencing MRI contrast, such as vessels and neurons.

3D dMRI/SXRPT CO-REGISTRATION METHOD OF THE MOUSE CNS

Here, we briefly describe a pipeline to co-register dMRI and SXRPT data from the C57BL/6J mouse brain and spinal cord acquired from the same animal (**Figure 2**). *Ex vivo* DTI was acquired with a 9.4 T scanner using segmented spin-echo EPI (TE = 32 ms, TR = 1 s, *b*-value = 3000 s/mm (Filippi and Rocca, 2004), 42 diffusion directions, and 125 μm -isotropic resolution). We generated fractional anisotropy (FA) and directionally encoded colored maps. SXRPT data was acquired at ID17 beamline at the European Synchrotron Radiation Facility (ESRF) in Grenoble, France. Free-space propagation method, beam energy = 34 keV, CCD pixel size = 3 μm , detector-sample distance \approx 2.3 m, and samples loaded in a cell filled with agar-agar were used. As the different 3D imaging techniques require different holders, the curvature of the images may differ from each other to an unknown degree. We propose two potential solutions to the



co-registration problem. In the first approach, we segmented 3D images acquired with both techniques, co-registered the images to each other, and fine-tuned using non-linear co-registration tools such as SyN (Avants et al., 2008). This approach works as long as the curvature of the images acquired by MRI and SXPCT is reasonably similar. While this assumption is generally true with brain samples, this is typically not the case for the spinal cord. This required the development of a second approach, wherein, first of all, we skeletonized both of the segmented images. The resulting skeletons were then straightened, and the image planes perpendicular to the skeletons were moved using the translations and rotations derived from the straightening process.

3D dMRI/SXPCT Co-registration Method of the Mouse Brain

First, SXPCT images were low pass filtered to avoid aliasing, and we down-sampled the images to roughly match the dMRI resolution [$125\ \mu\text{m}$ (Sled, 2018)]. Then, dMRI images were brain-masked using FSL's BET (Smith, 2002) on the B0 image (Figure 2D). Since no suitable tools for automatically masking SXPCT images are presently available, we used a combination of custom-made MATLAB routines for intensity thresholding, morphological operations, and manual fine-tuning for this task. The brain boundaries showed marginal ring artifacts due to different material density at the interface. An initial brain outline

mask was produced using intensity thresholding and including low and high intensities into the mask to reduce the artifact. The mask was then dilated with a 3D circle-shaped structuring element (MATLAB imdilate; radius = 2 voxels) to close the borders and hole-filled using 2D operations (MATLAB-imfill) on the single slices. This was followed by erosions (MATLAB-imerode) with the 3D ball-shaped structuring element until parts of the mask outside of the brain disappeared. The mask was finally dilated to reach the edges of the brain volume (Figure 2E). Since FA contrast resembled the contrast in SXPCT images in some regions, such as the corpus callosum, hippocampus proper and ventricles, we were able to co-register the FA images to the corresponding SXPCT using advanced normalization tools (ANTs) (Avants et al., 2009). In addition to affine co-registration, we used non-linear diffeomorphic registration SyN (Avants et al., 2008) with Mattes metric (Figure 2F) to compensate for possible small sample alterations due to different preparations and susceptibility-induced distortions in the dMRI imaging.

Our analysis yielded a good anatomical agreement between dMRI and SXPCT images after co-registration. After the 3D co-registration, the native resolution of SXPCT images can be restored allowing a more advanced analysis and validation of the dMRI maps.

Therefore, a 3D high-resolution micro-imaging technique is required in order to delineate simultaneously the complex vascular organization, down to the smallest capillaries, and the

neuronal and axonal morphology in a large volume of tissue (i.e., the same volume of the MRI scanning) This is a fundamental step toward a better understanding of the neuro-vascular coupling.

3D dMRI/SXPCT Co-registration of the Mouse Spinal Cord

While existing co-registration tools could be used for the brain, they do not work for the spinal cord and different template and toolbox have been proposed (De Leener et al., 2017; Cohen-Adad, 2018). The geometry of spinal cord requires more sophisticated tools to co-register datasets into the same reference frame, and in particular the coarse invariance for axial translations is a significant challenge for proper co-registration. Therefore, we devised a potential strategy, as described below, based on a combination of MATLAB routines to obtain a good quality co-registration between dMRI and SXPCT images of the spinal cord. Since the bones, i.e., vertebrae, were removed prior to the imaging, the location of the intervertebral discs based on image intensity was not possible. Therefore, both the SXPCT and dMRI data were manually labeled at two consensus reference coordinates, e.g., close to the sample's extremities. These reference points were necessary to insert the images of the two different modalities in the same space, regardless of the image resolution. We use the spinal cord toolbox (SCT) (De Leener et al., 2017) for spinal cord straightening (Figures 2I,J).

Synchrotron X-ray phase contrast tomography images were first intensity-adjusted saturating top and bottom 0.3% and down-sampled using volumetric nearest-neighbor interpolation (Figure 2). The scaling value for down-sampling was chosen to maximize the image gradient at the sample-medium interface on selected slices in the xy-plane. Then, the contours of the spinal cord were determined in the volume using the “approximate Canny method” for 3D-edge-detection (Canny, 1987) (the approximate Canny method uses two thresholds to detect strong and weak edges). Image intensity threshold was calculated using Otsu's method (Otsu, 1979). Two different approaches were used to determine the spinal cord position on the SXPCT images. The first was based on the center of mass of contour images determined on slices in the xy-plane, which yielded spinal cord centerlines. The second was based on filling of edge images using three-dimensional seeded region growing, which yielded spinal cord binary masks. The original SXPCT stack and either the spinal cord centerline or the binary mask were then fed to the SCT straightening algorithm (De Leener et al., 2017). The SXPCT binary mask and DTI images were finally then co-registered using ANTs (Figures 2K,L). This approach can be especially useful with parametric maps derived in the original image reference frames that could be transformed into the straightened form. This approach is also robust with respect to different curvatures in the images and, most importantly, it allows us to place all the spinal cord images from different individuals into the same reference frame. In addition, with XRPCT it is also possible to extract information simultaneously about the neuronal and vascular networks.

The potential outcomes of advancing these methods are great, enhancing our basic understanding of healthy human CNS

function, and improving our ability to accurately diagnose and treat injury and disease and predict treatment outcomes.

The co-registration methods presented here open new possibilities to obtain complementary information to validate MRI. Future directions are to include other histological modalities, as 3D LM or EM data as well as other MRI modalities, into the pipeline. Also, new analysis methods, such as segmentation and quantification of individual cellular components (Abdollahzadeh et al., 2019a,b; Figure 2L), allow to extract more specific morphological information for the evaluation of areas under investigation. A multiscale and multidisciplinary approach as proposed in this article paves new ways to study the brain and spinal cord, and more importantly, to better understand the non-invasive information given by *in vivo* MRI.

DISCUSSION

Magnetic resonance imaging has become one of the most powerful tools in neuroscience research, with a wide range of applications in both clinical practice and research settings. However, the interpretation of highly complex MRI contrasts remains a daunting task, which would benefit tremendously from the progress of multimodal and multiscale imaging approaches.

Synchrotron X-ray phase contrast tomography, LM, or EM can perform 3D imaging of post-mortem CNS tissue displaying, e.g., from the architecture of the neuronal and vascular network up to a single neuronal soma. These methods can be useful to validate *in vivo* imaging techniques using the high-resolution images as a reference (Schulz et al., 2012; Gangolli et al., 2017; Cohen-Adad, 2018). In particular, LM and EM offer high-resolution and specificity to visualize different cellular substrates, which have already exploited for the microstructural MRI validation (Mac Donald et al., 2007; Budde et al., 2011; Salo et al., 2017; Cohen-Adad, 2018; Duval et al., 2019). In the recent years, LM and EM have been developed into 3D imaging techniques generating new ways for the MRI validation (Khan et al., 2015; Schilling et al., 2016, 2018; Salo et al., 2018; Lee et al., 2019). On the other hand, SXPCT offers the possibility to study the tissue in 3D without sample sectioning and specific sample preparation (Fitzgerald, 2000). SXPCT allows both the assessment of the overall 3D morphology of the sample and fine computing sectioning, as thin as 130 nm. SXPCT has been applied in the imaging of the 3D distribution of vasculature and the single elements of the neuronal network in healthy and pathological CNS (Bravin et al., 2012; Stefanutti et al., 2018). The combination of the MRI with high-resolution SXPCT can, in principle, allow the assessment of the tissue morphology and the segmentation of different anatomical structures (Schulz et al., 2012) thus permitting to shed light on pathological alterations.

Co-registration methods, as the one presented here, allow to gather information from complementary imaging methods at different length scales spanning from the macroscopic to the nanometric level. The application of these techniques to *ex vivo* brain and spinal cord, for example, allows quantifying microstructural alterations in diseased subjects, and it has the

potential to lead to a better understanding of the relationship between structure and function in the CNS. One of the major limitations of the co-registration using different imaging modalities on the same sample is the tissue preparation (Fitzgerald, 2000). In this work, the tissue was fixed with paraformaldehyde, which only induces a minor tissue shrinkage. Other methods, such as LM or EM, require that the tissue be stained, resulting in a more significant shrinkage that can complicate the co-registration process. Prospectively, the added value of a multimodal and multiscale imaging can be greatly increased by further improvements in co-registration approaches such as those outlined here.

DATA AVAILABILITY STATEMENT

The raw data supporting the conclusions of this article will be made available by the authors, without undue reservation, to any qualified researcher.

ETHICS STATEMENT

All animal procedures were carried out under licenses that have been approved by the Animal Ethics Committee of the Provincial

Government of Southern Finland and in accordance with the guidelines of the European Community Council Directives 86/609/EEC.

AUTHOR CONTRIBUTIONS

MF and AS contributed to the concept and study design. AA, MD, RS, and LM performed the analyses. All authors have contributed to the interpretation the data, wrote the main manuscript text, and reviewed the manuscript.

ACKNOWLEDGMENTS

We thank Academy of Finland (AS #284544, #275453; OG #298007; JT #316258), COST Action CA15124 (NEUBIAS) (RS), and the Italian Ministry of Health under the Young Researcher Grant 2013 (GR-2013-02358177) for the financial support. In addition, part of the project was founded by the Progetto FISR – C.N.R. Tecnopolo di Nanotecnologia e Fotonica per la Medicina di Precisione and by the European Union Horizon 2020 Research and Innovation Program under the Marie Skłodowska-Curie grant agreement no. 691110 (MICROBRADAM).

REFERENCES

- Abdollahzadeh, A., Belevich, I., Jokitalo, E., Sierra, A., and Tohka, J. (2019a). DeepACSON: automated segmentation of white matter in 3D electron microscopy. *bioRxiv [Preprint]* doi: 10.1101/828541
- Abdollahzadeh, A., Belevich, I., Jokitalo, E., Tohka, J., and Sierra, A. (2019b). Automated 3D axonal morphometry of white matter. *Sci. Rep.* 9:6084. doi: 10.1038/s41598-019-42648-2
- Aggarwal, M., Li, X., Gröhn, O., and Sierra, A. (2018). Nuclei-specific deposits of iron and calcium in the rat thalamus after status epilepticus revealed with quantitative susceptibility mapping (QSM). *J. Magn. Reson. Imaging* 47, 554–564. doi: 10.1002/jmri.25777
- Andre, J. B., and Bammer, R. (2010). Advanced diffusion-weighted magnetic resonance imaging techniques of the human spinal cord. *Top. Magn. Reson. Imaging* 21, 367–378. doi: 10.1097/rmr.0b013e31823e65a1
- Avants, B. B., Epstein, C. L., Grossman, M., and Gee, J. C. (2008). Symmetric diffeomorphic image registration with cross-correlation: evaluating automated labeling of elderly and neurodegenerative brain. *Med. Image Analysis* 12, 26–41. doi: 10.1016/j.media.2007.06.004
- Avants, B. B., Tustison, N., and Song, G. (2009). Advanced normalization tools (ANTS). *Insight J.* 2, 1–35.
- Basser, P. J., Mattiello, J., and LeBihan, D. (1994). MR diffusion tensor spectroscopy and imaging. *Biophys. J.* 66, 259–267. doi: 10.1016/s0006-3495(94)80775-1
- Bravin, A., Coan, P., and Suortti, P. (2012). X-ray phase-contrast imaging: from pre-clinical applications towards clinics. *Phys. Med. Biol.* 58:R1. doi: 10.1088/0031-9155/58/1/R1
- Briggman, K. L., and Bock, D. D. (2012). Volume electron microscopy for neuronal circuit reconstruction. *Curr. Opin. Neurobiol.* 22, 154–161. doi: 10.1016/j.conb.2011.10.022
- Budde, M. D., Janes, L., Gold, E., Turtzo, L. C., and Frank, J. A. (2011). The contribution of gliosis to diffusion tensor anisotropy and tractography following traumatic brain injury: validation in the rat using Fourier analysis of stained tissue sections. *Brain* 134, 2248–2260. doi: 10.1093/brain/awr161
- Canny, J. (1987). *A Computational Approach to Edge Detection. Readings in Computer Vision*. Amsterdam: Elsevier, 184–203.
- Cedola, A., Bravin, A., Bukreeva, I., Fratini, M., Pacureanu, A., Mittone, A., et al. (2017). X-ray phase contrast tomography reveals early vascular alterations and neuronal loss in a multiple sclerosis model. *Sci. Rep.* 7:5890. doi: 10.1038/s41598-017-06251-7
- Chung, K., Wallace, J., Kim, S.-Y., Kalyanasundaram, S., Andalman, A. S., Davidson, T. J., et al. (2013). Structural and molecular interrogation of intact biological systems. *Nature* 497, 332–337. doi: 10.1038/nature12107
- Cohen, Y., Anaby, D., and Morozov, D. (2017). Diffusion MRI of the spinal cord: from structural studies to pathology. *NMR Biomed.* 30:e3592. doi: 10.1002/nbm.3592
- Cohen, Y., and Assaf, Y. (2002). High b-value q-space analyzed diffusion-weighted MRS and MRI in neuronal tissues—a technical review. *NMR Biomed.* 15, 516–542. doi: 10.1002/nbm.778
- Cohen-Adad, J. (2018). Microstructural imaging in the spinal cord and validation strategies. *Neuroimage* 182, 169–183. doi: 10.1016/j.neuroimage.2018.04.009
- De Leener, B., Lévy, S., Dupont, S. M., Fonov, V. S., Stikov, N., Collins, D. L., et al. (2017). SCT: spinal cord toolbox, an open-source software for processing spinal cord MRI data. *Neuroimage* 145, 24–43. doi: 10.1016/j.neuroimage.2016.10.009
- Denk, W., and Horstmann, H. (2004). Serial block-face scanning electron microscopy to reconstruct three-dimensional tissue nanostructure. *PLoS Biol.* 2:e329. doi: 10.1371/journal.pbio.0020329
- Denk, W., Strickler, J. H., and Webb, W. W. (1990). Two-photon laser scanning fluorescence microscopy. *Science* 248, 73–76. doi: 10.1126/science.2321027
- Du, H., Hou, P., Zhang, W., and Li, Q. (2018). Advances in CLARITY-based tissue clearing and imaging. *Exp. Ther. Med.* 16, 1567–1576.
- Duval, T., Salianni, A., Nami, H., Nanci, A., Stikov, N., Leblond, H., et al. (2019). Axons morphometry in the human spinal cord. *Neuroimage* 185, 119–128. doi: 10.1016/j.neuroimage.2018.10.033
- Ertürk, A., and Bradke, F. (2013). High-resolution imaging of entire organs by 3-dimensional imaging of solvent cleared organs (3DISCO). *Exp. Neurol.* 242, 57–64. doi: 10.1016/j.expneurol.2012.10.018
- Filippi, M., and Rocca, M. A. (2004). Magnetization transfer magnetic resonance imaging in the assessment of neurological diseases. *J. Neuroimaging* 14, 303–313. doi: 10.1111/j.1552-6569.2004.tb00255.x
- Filippi, M., and Rocca, M. A. (2007). Magnetization transfer magnetic resonance imaging of the brain, spinal cord, and optic nerve. *Neurotherapeutics* 4, 401–413. doi: 10.1016/j.nurt.2007.03.002

- Fitzgerald, R. (2000). Phase-sensitive x-ray imaging. *Phys. Today* 53, 23–26. doi: 10.1063/1.1292471
- Fratini, M. (2018). “The challenge of the vascularization of regenerated tissues,” in *Advanced High-Resolution Tomography in Regenerative Medicine: Three-Dimensional Exploration into the Interactions between Tissues, Cells, and Biomaterials*, eds A. Giuliani, and A. Cedola, (Cham: Springer), 139. doi: 10.1007/978-3-030-00368-5_9
- Fratini, M., Bukreeva, I., Campi, G., Brun, F., Tromba, G., Modregger, P., et al. (2015). Simultaneous submicrometric 3D imaging of the micro-vascular network and the neuronal system in a mouse spinal cord. *Sci. Rep.* 5:8514.
- Gangolli, M., Holleran, L., Kim, J. H., Stein, T. D., Alvarez, V., McKee, A. C., et al. (2017). Quantitative validation of a nonlinear histology-MRI coregistration method using generalized Q-sampling imaging in complex human cortical white matter. *Neuroimage* 153, 152–167. doi: 10.1016/j.neuroimage.2017.03.059
- Gustafsson, M. G. (2000). Surpassing the lateral resolution limit by a factor of two using structured illumination microscopy. *J. Microsc.* 198, 82–87. doi: 10.1046/j.1365-2818.2000.00710.x
- Hama, H., Hioki, H., Namiki, K., Hoshida, T., Kurokawa, H., Ishidate, F., et al. (2015). ScaleS: an optical clearing palette for biological imaging. *Nat. Neurosci.* 18, 1518–1529. doi: 10.1038/nn.4107
- Hell, S. W., and Wichmann, J. (1994). Breaking the diffraction resolution limit by stimulated emission: stimulated-emission-depletion fluorescence microscopy. *Opt. Lett.* 19, 780–782.
- Helmstaedter, M., Briggman, K. L., and Denk, W. (2008). 3D structural imaging of the brain with photons and electrons. *Curr. Opin. Neurobiol.* 18, 633–641. doi: 10.1016/j.conb.2009.03.005
- Heymann, J. A., Hayles, M., Gestmann, I., Giannuzzi, L. A., Lich, B., and Subramaniam, S. (2006). Site-specific 3D imaging of cells and tissues with a dual beam microscope. *J. Struct. Biol.* 155, 63–73. doi: 10.1016/j.jsb.2006.03.006
- Jensen, J. H., Helpert, J. A., Ramani, A., Lu, H., and Kaczynski, K. (2005). Diffusional kurtosis imaging: the quantification of non-gaussian water diffusion by means of magnetic resonance imaging. *Magn. Reson. Med.* 53, 1432–1440. doi: 10.1002/mrm.20508
- Khan, A. R., Cornea, A., Leigland, L. A., Kohama, S. G., Jespersen, S. N., and Kroenke, C. D. (2015). 3D structure tensor analysis of light microscopy data for validating diffusion MRI. *Neuroimage* 111, 192–203. doi: 10.1016/j.neuroimage.2015.01.061
- Kreshuk, A., Koethe, U., Pax, E., Bock, D. D., and Hamprecht, F. A. (2014). Automated detection of synapses in serial section transmission electron microscopy image stacks. *PLoS One* 9:e87351. doi: 10.1371/journal.pone.0087351
- Lee, H.-H., Yaros, K., Veraart, J., Pathan, J. L., Liang, F.-X., Kim, S. G., et al. (2019). Along-axon diameter variation and axonal orientation dispersion revealed with 3D electron microscopy: implications for quantifying brain white matter microstructure with histology and diffusion MRI. *Brain Struct. Funct.* 224, 1469–1488. doi: 10.1007/s00429-019-01844-6
- Li, X., Harrison, D. M., Liu, H., Jones, C. K., Oh, J., Calabresi, P. A., et al. (2016). Magnetic susceptibility contrast variations in multiple sclerosis lesions. *J. Magn. Reson. Imaging* 43, 463–473. doi: 10.1002/jmri.24976
- Liu, C., Li, W., Tong, K. A., Yeom, K. W., and Kuzminski, S. (2015). Susceptibility-weighted imaging and quantitative susceptibility mapping in the brain. *J. Magn. Reson. Imaging* 42, 23–41. doi: 10.1002/jmri.24768
- Mac Donald, C., Dikranian, K., Song, S., Bayly, P., Holtzman, D., and Brody, D. (2007). Detection of traumatic axonal injury with diffusion tensor imaging in a mouse model of traumatic brain injury. *Exp. Neurol.* 205, 116–131. doi: 10.1016/j.expneurol.2007.01.035
- Massimi, L., Bukreeva, I., Santamaria, G., Fratini, M., Corbelli, A., Brun, F., et al. (2019). Exploring Alzheimer's disease mouse brain through X-ray phase contrast tomography: from the cell to the organ. *Neuroimage* 184, 490–495. doi: 10.1016/j.neuroimage.2018.09.044
- Mezer, A., Rokem, A., Bertram, S., Hastie, T., and Wandell, B. A. (2016). Evaluating quantitative proton-density-mapping methods. *Hum. Brain Mapp.* 37, 3623–3635. doi: 10.1002/hbm.23264
- Otsu, N. (1979). A threshold selection method from gray-level histograms. *IEEE Trans. Syst. Man Cybern.* 9, 62–66. doi: 10.1109/tsmc.1979.4310076
- Paganin, D., Mayo, S., Gureyev, T. E., Miller, P. R., and Wilkins, S. W. (2002). Simultaneous phase and amplitude extraction from a single defocused image of a homogeneous object. *J. Microsc.* 206, 33–40. doi: 10.1046/j.1365-2818.2002.01010.x
- Panagiotaki, E., Schneider, T., Siow, B., Hall, M. G., Lythgoe, M. F., and Alexander, D. C. (2012). Compartment models of the diffusion MR signal in brain white matter: a taxonomy and comparison. *Neuroimage* 59, 2241–2254. doi: 10.1016/j.neuroimage.2011.09.081
- Russo, P. (2017). *Handbook of X-ray Imaging: Physics and Technology*. Boca Raton, FL: CRC Press.
- Salo, R. A., Belevich, I., Manninen, E., Jokitalo, E., Gröhn, O., and Sierra, A. (2018). Quantification of anisotropy and orientation in 3D electron microscopy and diffusion tensor imaging in injured rat brain. *Neuroimage* 172, 404–414. doi: 10.1016/j.neuroimage.2018.01.087
- Salo, R. A., Miettinen, T., Laitinen, T., Gröhn, O., and Sierra, A. (2017). Diffusion tensor MRI shows progressive changes in the hippocampus and dentate gyrus after status epilepticus in rat—histological validation with Fourier-based analysis. *Neuroimage* 152, 221–236. doi: 10.1016/j.neuroimage.2017.03.003
- Schalek, R., Kasthuri, N., Hayworth, K., Berger, D., Tapia, J., Morgan, J., et al. (2011). Development of high-throughput, high-resolution 3D reconstruction of large-volume biological tissue using automated tape collection ultramicrotomy and scanning electron microscopy. *Microsc. Microanal.* 17, 966–967. doi: 10.1017/s1431927611005708
- Schilling, K., Janve, V., Gao, Y., Stepniewska, I., Landman, B. A., and Anderson, A. W. (2016). Comparison of 3D orientation distribution functions measured with confocal microscopy and diffusion MRI. *Neuroimage* 129, 185–197. doi: 10.1016/j.neuroimage.2016.01.022
- Schilling, K. G., Janve, V., Gao, Y., Stepniewska, I., Landman, B. A., and Anderson, A. W. (2018). Histological validation of diffusion MRI fiber orientation distributions and dispersion. *Neuroimage* 165, 200–221. doi: 10.1016/j.neuroimage.2017.10.046
- Schulz, G., Waschkies, C., Pfeiffer, F., Zanette, I., Weitkamp, T., David, C., et al. (2012). Multimodal imaging of human cerebellum—merging X-ray phase microtomography, magnetic resonance microscopy and histology. *Sci. Rep.* 2:826. doi: 10.1038/srep00826
- Schweser, F., Deistung, A., Lehr, B. W., and Reichenbach, J. R. (2011). Quantitative imaging of intrinsic magnetic tissue properties using MRI signal phase: an approach to in vivo brain iron metabolism? *Neuroimage* 54, 2789–2807. doi: 10.1016/j.neuroimage.2010.10.070
- Sled, J. G. (2018). Modelling and interpretation of magnetization transfer imaging in the brain. *Neuroimage* 182, 128–135. doi: 10.1016/j.neuroimage.2017.11.065
- Smith, S. M. (2002). Fast robust automated brain extraction. *Hum. Brain Mapp.* 17, 143–155. doi: 10.1002/hbm.10062
- Stefanutti, E., Sierra, A., Miocchi, P., Massimi, L., Brun, F., Maugeri, L., et al. (2018). Assessment of the effects of different sample perfusion procedures on phase-contrast tomographic images of mouse spinal cord. *J. Instrum.* 13:C03027.
- Stelzer, E. H. (2006). “The intermediate optical system of laser-scanning confocal microscopes,” in *Handbook of Biological Confocal Microscopy*, ed. J. B. Pawley, (Berlin: Springer), 207–220. doi: 10.1007/978-0-387-45524-2_9
- Topgaard, D. (2017). Multidimensional diffusion MRI. *J. Magn. Reson.* 275, 98–113. doi: 10.1016/j.jmr.2016.12.007
- Tuch, D. S., Reese, T. G., Wiegell, M. R., Makris, N., Belliveau, J. W., and Wedeen, V. J. (2002). High angular resolution diffusion imaging reveals intravoxel white matter fiber heterogeneity. *Magn. Reson. Med.* 48, 577–582. doi: 10.1002/mrm.10268
- Vargas, M., Delattre, B., Boto, J., Gariani, J., Dhoub, A., Fittsiori, A., et al. (2018). Advanced magnetic resonance imaging (MRI) techniques of the spine and spinal cord in children and adults. *Insights Imaging* 9, 549–557. doi: 10.1007/s13244-018-0626-1
- Wang, Y., and Liu, T. (2015). Quantitative susceptibility mapping (QSM): decoding MRI data for a tissue magnetic biomarker. *Magn. Reson. Med.* 73, 82–101. doi: 10.1002/mrm.25358
- Weber, M., and Huisken, J. (2011). Light sheet microscopy for real-time developmental biology. *Curr. Opin. Genet. Dev.* 21, 566–572. doi: 10.1016/j.gde.2011.09.009
- Wedeen, V. J., Wang, R., Schmahmann, J. D., Benner, T., Tseng, W.-Y. I., Dai, G., et al. (2008). Diffusion spectrum magnetic resonance imaging (DSI) tractography of crossing fibers. *Neuroimage* 41, 1267–1277. doi: 10.1016/j.neuroimage.2008.03.036

- Weitkamp, T., Haas, D., Wegrzynek, D., and Rack, A. (2011). ANKAphase: software for single-distance phase retrieval from inline X-ray phase-contrast radiographs. *J. Synchrotron Radiat.* 18, 617–629. doi: 10.1107/S0909049511002895
- Westin, C.-F., Knutsson, H., Pasternak, O., Szczepankiewicz, F., Özarlan, E., van Westen, D., et al. (2016). Q-space trajectory imaging for multidimensional diffusion MRI of the human brain. *Neuroimage* 135, 345–362. doi: 10.1016/j.neuroimage.2016.02.039
- Zhang, H., Schneider, T., Wheeler-Kingshott, C. A., and Alexander, D. C. (2012). NODDI: practical in vivo neurite orientation dispersion and density imaging of the human brain. *Neuroimage* 61, 1000–1016. doi: 10.1016/j.neuroimage.2012.03.072

Conflict of Interest: The authors declare that the research was conducted in the absence of any commercial or financial relationships that could be construed as a potential conflict of interest.

Copyright © 2020 Fratini, Abdollahzadeh, DiNuzzo, Salo, Maugeri, Cedola, Giove, Gröhn, Tohka and Sierra. This is an open-access article distributed under the terms of the Creative Commons Attribution License (CC BY). The use, distribution or reproduction in other forums is permitted, provided the original author(s) and the copyright owner(s) are credited and that the original publication in this journal is cited, in accordance with accepted academic practice. No use, distribution or reproduction is permitted which does not comply with these terms.